Available online at www.sciencedirect.com
SCIENCE DIRECT®
PERGAMON
International Journal of Heat and Mass Transfer 46 (2003) 1359–1369
International Journal of HEAT and MASS TRANSFER
www.elsevier.com/locate/ijhmt

Fully developed electro-osmotic heat transfer in microchannels

D. Maynes, B.W. Webb *

Department of Mechanical Engineering, Brigham Young University, 435 CTB, Provo, UT 84602, USA

Received 16 April 2002; received in revised form 27 September 2002

Abstract

Thermally fully developed, electro-osmotically generated convective transport has been analyzed for a parallel plate microchannel and circular microtube under imposed constant wall heat flux and constant wall temperature boundary conditions. Such a flow is established not by an imposed pressure gradient, but by a voltage potential gradient along the length of the tube. The result is a combination of unique electro-osmotic velocity profiles and volumetric heating in the fluid due to the imposed voltage gradient. The exact solution for the fully developed, dimensionless temperature profile and corresponding Nusselt number have been determined analytically for both geometries and both thermal boundary conditions. The fully developed temperature profiles and Nusselt number are found to depend on the relative duct radius (ratio of the Debye length to duct radius or plate gap half-width) and the magnitude of the dimensionless volumetric source.

1. Introduction

Microfluidic transport has found importance in a number of emerging technologies in micropower generation, chemical separation processes, cell analysis and other biomedical diagnostic techniques. At physical scales of order 100 μm, generating fluid motion in the tube poses a considerable challenge. Conventional pressure-driven flow technology requires significant pressures, and while micropumps exist which are capable of delivering such pressures [1–3], they are difficult to manufacture and maintain [1], and lack the precise control that is often needed in microfluidic applications [4]. Electro-osmotic flow may provide a viable alternative to pressure-driven liquid flow at the microscale, with better flow control and no moving parts, and several investigators have reported on electro-osmotic pump systems [5–9].

Electro-osmosis is the bulk movement of liquid relative to a stationary surface due to an externally applied electric field, and was first observed and reported by Reuss nearly two centuries ago [10]. Most solid substances will acquire a relative electric charge when in contact with an aqueous (polar) solution, which influences the charge distribution in the solution. Ions of opposite charge (counterions) to that of the surface are attracted towards the surface and ions of the same charge (coions) are repelled from the surface as shown in Fig. 1a. The net effect is the formation of a region close to the charged surface called the electric double layer (EDL) in which there is an excess of counterions over coions, and which are distributed in a diffuse manner [11]. The charge distribution in the fluid therefore falls from its maximum near the wall (characterized by the zeta potential) to a zero charge in the fluid core (for large enough tube radius). The thickness of this layer is characterized by the Debye length, which is the distance over which the net charge has decreased from the charge magnitude near the tube wall surface to $1/e$ (37%) of the surface charge. For example, glass and fused silica capillaries carry dissociable silanol groups on the surface, and are therefore negatively charged when

* Corresponding author. Tel.: +1-801-378-6543; fax: +1-801-378-5037.
E-mail address: webb@byu.edu (B.W. Webb).

0017-9310/03/$ - see front matter © 2002 Elsevier Science Ltd. All rights reserved.
PII: S0017-9310(02)00423-4

Nomenclature

a	tube radius or channel gap half-width
C	fluid specific heat
D_h	hydraulic diameter
h	convective heat transfer coefficient
i_e	conduction current density
k	thermal conductivity
k_b	Boltzmann constant
Nu	Nusselt number (hD_h/k)
Pe	Peclet number $(RePr)$
Pr	Prandtl number (v/α)
r	radial coordinate
R	normalized radial coordinate (r/a)
Re	Reynolds number $(\rho\bar{u}D/\mu)$
q''_w	wall heat flux
s	volumetric energy generation
S	normalized energy generation
T	absolute temperature
T_m	mixed mean temperature
T_w	channel wall temperature
u	local fluid velocity
u_{max}	maximum possible electro-osmotic velocity
$\bar{u}$	average velocity
U	normalized local velocity $(u/\bar{u})$
$\overline{U}_{max}$	ratio of mean velocity to maximum electro-osmotic velocity
x	streamwise coordinate
x_{fd}	fully developed distance
y	wall-normal coordinate
Y	normalized wall-normal coordinate (y/a)
Z	ratio of tube radius (or plate gap half-width) to Debye length

Greek symbols

α	thermal diffusivity
ε	fluid dielectric constant
Φ	applied potential field
μ	absolute viscosity
v	kinematic viscosity
ρ	fluid density
σ	liquid electrical resistivity
θ	normalized temperature
θ_w	normalized wall temperature
ψ	excess charge distribution
ζ	wall zeta potential

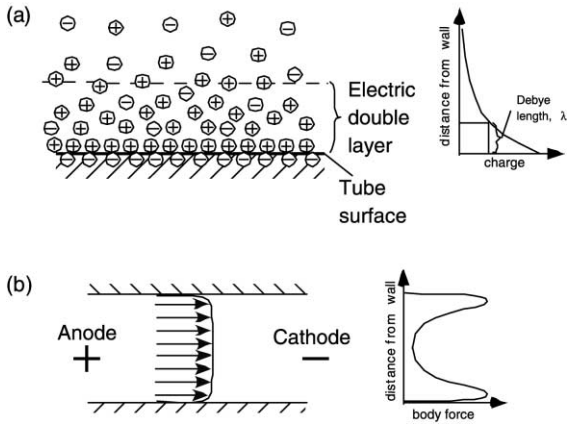

Fig. 1. Schematic illustration of electro-osmotically generated flow.

adjacent to polar liquids. The positively charged cations and solvent molecules strongly adsorbed at the wall will remain stationary under the influence of an electric potential in the streamwise direction. However, the mobile cations in the EDL very near the tube walls will migrate toward the cathode due to the excess charge in the layer, which gives rise to a fluid body force near the tube walls as illustrated in Fig. 1b. Viscous shear forces transmitted from the EDL to the tube center pull the core fluid towards the cathode as well. The resulting electro-osmotic flow velocity distribution is a function of the ratio of the Debye length to the capillary hydraulic radius. When the Debye length is much less than the capillary radius, the resulting velocity profile is nearly flat (characterized by slug flow). At the other extreme, when the Debye length is of the same order as the capillary radius, the flow exhibits velocity gradients normal to the tube wall with a maximum in velocity near the tube centerline (i.e., velocity distribution more nearly like that of classical pressure-driven flow). Of course, the total electro-osmotic flow rate in the tube is a function of the electro-osmotic characteristics of the tube/fluid combination (electro-osmotic mobility), tube size, imposed voltage potential, etc. Generally speaking, the total flow rate in the tube is inversely related to the Debye length.

Since the fluid dynamics of electro-osmotically generated flow are significantly different from traditional pressure-driven flow, the thermal transport dynamics are expected to be quite different as well. Two elements of electro-osmotically generated flow result in departure from traditional pressure-driven flow heat transfer. First, the velocity profile in the tube will be a strong function of the electro-osmotic character of the flow, described by the electro-osmotic mobility and applied voltage gradient along the tube length. These parameters affect the magnitude of the electro-osmotically induced flow, but assuming no variation in the liquid viscosity,

dielectric constant, and wall zeta potential, the shape of the velocity profile is dependent only on the ratio of the channel dimension to Debye length. The electro-osmotically generated velocity profile in the tube will influence the temperature distribution and resulting heat transfer. Second, the applied voltage gradient and its induced electric conduction current establishes Joule heating in the fluid, resulting in volumetric energy generation therein. The magnitude of the thermal energy source has significant influence on the temperature distribution and heat transfer.

For the case of electro-osmotic flow in microtubes with small Debye length, near-slug flow will prevail. Laminar, thermally developing transport in a circular tube under slug flow velocity conditions has been previously analyzed [12]. The thermal entrance region for slug flow in a circular tube is considerably longer than for pressure-driven flow (with its resulting parabolic velocity profile), and is given by $x_{fd}/D_h \approx 0.25Pe$ where Pe is the Peclet number, equal to the product $RePr$. Hydrodynamically developing flow between parallel plates for electro-osmotically generated flow has also been reported in a numerical study by Yang et al. [13]. They also report that the hydrodynamic development length is about four times that associated with pressure-driven flow. Typical electro-osmotic flows feature low velocities on the order of a few mm/s, with resulting low Peclet numbers. For a typical electro-osmotic flow Peclet number of 100, slug flow yields a thermal development length of approximately 25 diameters. For a 100 μm tube, the thermal entry region is then approximately 2.5 mm in length. Thermally fully developed flow may thus prevail over the majority of the tube length. An understanding of the thermally fully developed transport characteristics for such flows is therefore needed.

Several analytical studies have appeared in the literature describing the hydrodynamics of fully developed electro-osmotic flow through circular and rectangular channels. Specifically, several early papers report on electro-osmotic velocity distributions and the associated momentum transport in capillaries as a function of channel diameter-to-Debye length ratio [14–16]. More recent hydrodynamic studies have explored the effects on the velocity field due to streamwise gradients in the electrical conductivity [17], the transient response of the velocity field to a suddenly applied voltage gradient [18], the entry region flow field development [13,19], and effects of variations in the wall zeta potential on the velocity profile characteristics [20,21]. Additionally, some experimental studies have reported on the velocity profile characteristics associated with fully developed electro-osmotic flow in very long circular and rectangular channels [22–27].

With regards to characterization of the convection heat transfer associated with electro-osmotic flow, relatively little prior work has appeared in the literature. Li et al. have explored electrokinetic effects induced in a pressure-driven flow on the frictional and heat transfer characteristics for both round and rectangular microchannels [28–30]. They report that the resulting induced electrokinetic potential results in a reduced flow rate, a greater friction factor, and a reduced Nusselt number from the classical laminar pressure-driven flow scenario. There also exists some early work exploring the effect of volumetric energy dissipation on thermal development in channels under pressure-driven flow conditions [31,32]. Other investigators have explored the influence of thermal band broadening due to Joule heating in capillary electrophoresis [33–35]. However, no studies have appeared in the literature that specifically address and describe the convective heat transport characteristics for purely electro-osmotically driven flow, with its unique combination of complex velocity distribution and fluid Joule heating. This study presents analytical solutions for thermally fully developed electro-osmotic flow in circular and parallel plate microchannels (based on previously reported velocity distributions) for both constant wall heat flux and constant wall temperature boundary conditions. The analysis assumes no pressure-driven component to the velocity field and constant conductivity (electrical and thermal). Also, the wall zeta potential is assumed be constant and less than $3k_bT$ such that the Debye–Hückel linearization holds [11]. The total electrical current drawn in electro-osmotically generated flow consists of two components, the so-called conduction and convection currents. Volumetric heating arises from the conduction current only and may be safely modeled using Ohm's law [15]. Further, this energy generation is distributed uniformly across the tube or channel cross-section for low zeta potential (as imposed here) or for large diameter-to-Debye length ratios [16].

Under the assumptions outlined above the convective heat transfer behavior is investigated parametrically for a range of problem scenarios relevant to electro-osmotic flow, including the full possible range of channel diameter-to-Debye length ratios.

2. Analysis

2.1. Momentum transport

Consider fully developed flow of an incompressible fluid in a microchannel (circular or rectangular of infinite width) where the flow is driven electro-osmotically with coordinates as shown in Fig. 2. For steady flow without an applied pressure gradient the streamwise momentum equation reduces to [11]

$$\mu \frac{1}{y^n}\frac{\mathrm{d}}{\mathrm{d}y}\left(y^n \frac{\mathrm{d}u}{\mathrm{d}y}\right) + \frac{\varepsilon}{y^n}\frac{\mathrm{d}}{\mathrm{d}y}\left(y^n \frac{\mathrm{d}\psi}{\mathrm{d}y}\right)\frac{\mathrm{d}\Phi}{\mathrm{d}x} = 0 \tag{1}$$

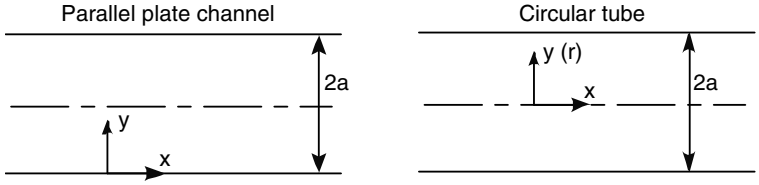

Fig. 2. Definition of coordinate system and dimensions for parallel plate channel and circular tube.

where $n = 0$ for the parallel plate configuration and $n = 1$ for the circular tube. μ and ε are the fluid viscosity and dielectric constant, respectively, and have been assumed to be constant in the present analysis. Φ is the applied potential field, and $\psi(y)$ is the excess charge distribution. For low wall potentials the Debye–Hückel linearization holds and the excess charge distribution is simply

$$\psi = \zeta e^{-y/\lambda} \quad (y \leqslant a) \tag{2}$$

for the parallel plate geometry [11], and

$$\psi = \zeta \frac{I_0(y/\lambda)}{I_0(a/\lambda)} \tag{3}$$

for the circular tube [14]. ζ is the zeta potential, or charge potential very near the wall, and is determined by the liquid–solid interfacial chemistry [11]. λ is the Debye length, a is the tube radius (or half the plate gap width), and I_0 is the modified Bessel function of the first kind of order zero. Upon substitution of Eq. (2) or (3) into Eq. (1), integrating twice, and applying boundary conditions reflecting no slip at the wall and zero shear stress at the centerline, the velocity distributions can be expressed for the parallel plate and circular tube, respectively, as

$$\frac{u}{u_{\max}} = [1 - e^{-Z} ZY - e^{-YZ}] \quad (Y \leqslant 1) \tag{4}$$

and

$$\frac{u}{u_{\max}} = \left[1 - \frac{I_0(ZR)}{I_0(Z)}\right] \tag{5}$$

$Y(= y/a)$ or R $(= r/a$ for the circular tube) is the non-dimensional wall-normal coordinate, and Z is the duct relative radius, or ratio of tube radius (or gap half-width) to the Debye length, a/λ. For large Z the size of the EDL or region of excess charge (and corresponding source of fluid momentum) is relatively small. Conversely, for $Z \to 1$ the double layer thickness is of the same order of magnitude as the channel radius and the region of excess charge (and source of fluid momentum) is distributed over the entire channel. The term $u_{\max} = (\varepsilon\zeta/\mu)\mathrm{d}\Phi/\mathrm{d}x$ represents the maximum possible electro-osmotic velocity for a given applied potential field, where $\varepsilon\zeta/\mu$ is often termed the electro-osmotic mobility of the liquid [36]. For large Z $(Z > 500)$ Eqs. (4) and (5) reduce to $u/u_{\max} = 1$ which is the classical Helmoltz-Smoluchowski equation [11]. Integration over the duct cross-sectional area yields the normalized average velocities expressed as

$$\overline{U}_{\max} = \frac{\bar{u}}{u_{\max}} = \left[1 - \frac{Ze^{-Z}}{2} + \frac{e^{-Z}}{Z} - \frac{1}{Z}\right] \tag{6}$$

and

$$\overline{U}_{\max} = \frac{\bar{u}}{u_{\max}} = \left[1 - \frac{2I_1(Z)}{ZI_0(Z)}\right] \tag{7}$$

for the two configurations, respectively.

The variation of $\overline{U}_{\max}$ with relative duct radius Z for the two duct geometries is shown in Fig. 3. Note that $\overline{U}_{\max}$ is greater for the parallel plate configuration than for the circular tube for all Z, and for $Z > 500$, $\overline{U}_{\max} \approx 1$. As the relative duct radius decreases, such that the double layer extends deeper into the core fluid, $\overline{U}_{\max}$ also decreases. In other words, the ratio of average velocity to maximum possible velocity for the applied potential field decreases as the excess charge distribution spreads over a larger portion of the duct. Profiles of the

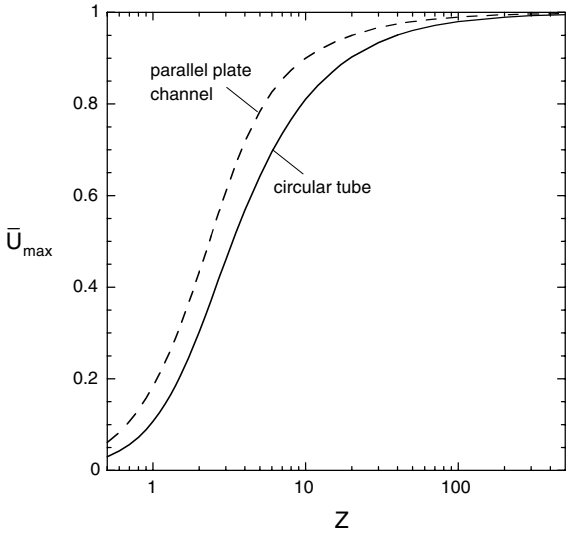

Fig. 3. Variation of electro-osmotically induced flow rate $\overline{U}_{\max}(= \bar{u}/u_{\max})$ as a function of Z for the parallel plate channel and the circular tube.

normalized local velocity, $U = u/\bar{u}$, are shown in Figs. 4 and 5 for the parallel plate and circular ducts, respectively, for Z varying between 0.5 and 100. For $Z \to \infty$, the velocity profiles exhibit slug-like behavior, with a very thin boundary layer. Conversely, as $Z \to 0.5$, the velocity profiles approach the classical parabolic distributions similar to Poiseuille flow, or gravity driven flows with uniform body force. At intermediate values of relative duct radius, where the source of momentum varies from a concentrated source near the duct walls ($Z > 100$) to a uniformly distributed source ($Z \to 0.5$) the velocity profiles change accordingly.

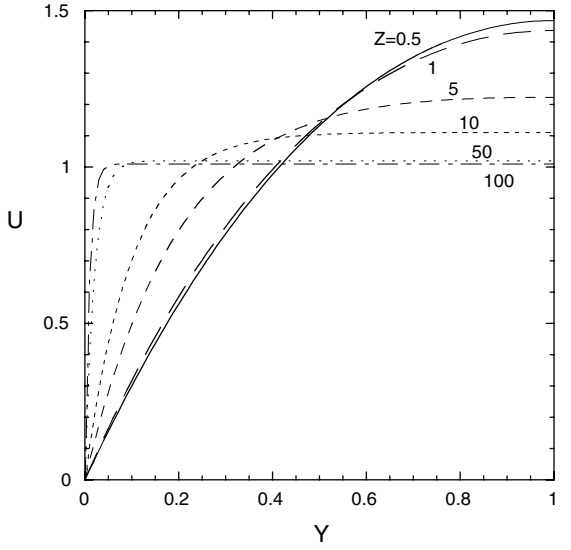

Fig. 4. Normalized electro-osmotically driven velocity profiles as a function of Z for the parallel plate channel.

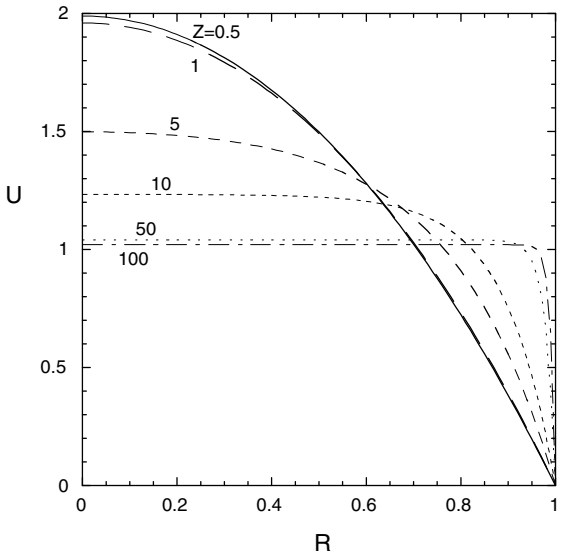

Fig. 5. Normalized electro-osmotically driven velocity profiles as a function of Z for the circular tube.

2.2. Thermal transport

2.2.1. Constant wall heat flux boundary condition

Given steady hydrodynamically fully developed flow with constant thermophysical properties, the energy equation simplifies to

$$\frac{\partial^2 T}{\partial x^2} + \frac{1}{y^n}\frac{\partial}{\partial y}\left(y^n \frac{\partial T}{\partial y}\right) = \frac{u}{\alpha}\frac{\partial T}{\partial x} - \frac{s}{k} \tag{8}$$

where n takes on the same values specified previously for the circular tube and parallel plate channel. T is the local temperature, α and k are the thermal diffusivity and conductivity, and s is the volumetric generation due to the resistance heating. For electro-osmotically driven flow, $s = i_e^2\sigma$ where i_e is the conduction current density (A/m^2) established by the applied potential and σ is the liquid electrical resistivity ($\Omega\,m$). If the flow field is also thermally fully developed, as defined by the classical definition of such

$$\frac{\partial}{\partial x}\left(\frac{T_w - T}{T_w - T_m}\right) = 0 \tag{9}$$

with an imposed constant heat flux boundary condition ($q''_w = \text{constant}$), $\partial T/\partial x = dT_m/dx = \text{constant}$, and $\partial^2 T/\partial x^2 = 0$. Furthermore, an energy balance on the fluid yields

$$\frac{dT_m}{dx} = \frac{4q''_w}{\rho \bar{u} C D_h} + \frac{s}{\rho \bar{u} C} \tag{10}$$

In the above, D_h is the hydraulic diameter, and ρ and C are the fluid density and specific heat, respectively. Substituting Eq. (10) into Eq. (8) and introducing the normalized temperature $\theta = (T - T_m)/(q''_w a/k)$, yields the nondimensional energy equation

$$\frac{1}{Y^n}\frac{d}{dY}\left(Y^n \frac{d\theta}{dY}\right) = \left(\frac{4a}{D_h} + S\right)U - S \tag{11}$$

where $S = sa/q''_w$ and $U = u/\bar{u}$. The associated boundary conditions are $d\theta/dY = 1$ at the wall and $d\theta/dY = 0$ at the centerline. In practice, one imposes $\theta_w = (T_w - T_m)/(q''_w a/k)$ at the wall, and integration of Eq. (11) twice results in an expression for θ in terms of θ_w. The unknown normalized wall temperature θ_w is then determined by evaluating the normalized mixed mean temperature from its definition:

$$\int_0^1 U(Y)\theta(Y)Y^n\,dY = 0 \tag{12}$$

Substituting the normalized velocity $U(Y)$ for electro-osmotic flow (for a particular value of Z), and the temperature $\theta(Y)$ from the solution of Eq. (11) subject to appropriate boundary conditions, the integral of Eq. (12) may be evaluated for θ_w. Substitution into the normalized temperature distribution results in an expression for θ as a function only of S, Z, and Y for each channel configuration. Despite their complexity, the expressions are included here for completeness. The dimensionless, fully developed temperature profile in the parallel plate channel is

$$\theta(Y) = \frac{(1+S)}{\overline{U}_{\max}}\left[F_1(Y,Z) - \frac{C_1(Z)}{\overline{U}_{\max}}\right] + S\left[\frac{C_2(Z)}{\overline{U}_{max}} - \left(\frac{Y^2}{2} - Y\right)\right] \tag{13}$$

The expression for the circular tube is (noting that $Y = R$ for this coordinate system)

$$\theta(R) = \left[\frac{2}{\overline{U}_{\max}} + S\left(\frac{1}{\overline{U}_{\max}} - 1\right)\right]\left[\frac{R^2-1}{4} + \frac{1}{8\overline{U}_{\max}}\right] + \frac{(2+S)}{Z^2\overline{U}_{\max}}\left[1 - \frac{I_0(ZR)}{I_0(Z)}\right] - \frac{(2+S)}{\overline{U}^2_{\max}}C_3(Z) + \frac{S}{\overline{U}_{\max}}C_4(Z) \tag{14}$$

Relations for $\overline{U}_{\max}$ as a function of relative duct radius Z were presented in Eqs. (6) and (7), respectively, for the parallel plate channel and circular tube. The remaining functions $F_1(Y,Z)$ and $C_i(Z)$ appearing in Eqs. (13) and (14) are listed in Table 1.

The Nusselt number is expressed generally as

$$Nu = \frac{q''_w D_h}{k(T_w - T_m)} = \frac{D_h}{a}\frac{1}{\theta_w} \tag{15}$$

and can now be determined in terms of S and Z by evaluating Eqs. (13) and (14) at the wall, $Y = 0$ and $R = 1$. After algebraic manipulation and rearrangement, the closed-form expression for the fully developed Nusselt number for the constant heat flux boundary for both the parallel plate channel and the circular tube may be cast in the form

$$Nu = \frac{\overline{U}^2_{\max}}{A(Z) + S\left(\frac{D_h}{4a}\right)B(Z)} \tag{16}$$

where again, expressions for $\overline{U}_{\max}$ are given in Eqs. (6) and (7) for the two channel geometries. The functions $A(Z)$ and $B(Z)$ depend only on the relative duct radius, and expressions are given in Table 2. As indicated previously, for large channels ($Z \to \infty$) the velocity becomes slug-like with magnitude equal to the maximum electro-osmotic velocity, and $\overline{U}_{\max} = 1$. The large-channel asymptotic values of $A(Z)$ for the parallel plate channel and circular tube are 1/12 and 1/8, respectively. The function $B(Z)$ vanishes at large Z for both geometries. Thus, for flows in large channels with $S \to 0$ (corresponding to no volumetric heating or very large imposed wall heat flux), the asymptotic values of the Nusselt number for the parallel plate and circular tube configurations are, respectively, $Nu = 12$ and $Nu = 8$. These values are identical to the classical slug flow results [12]. The Nusselt number dependence on S and Z

Table 1
Expressions for the functions in the fully developed temperature profiles, Eqs. (13) and (14)

Parallel plate channel

$$F_1(Y,Z) = \left(\frac{Y^2}{2} - Y\right) - \frac{Ze^{-Z}}{2}\left(\frac{Y^3}{3} - Y\right) - \frac{1}{Z^2}(e^{-YZ} + YZe^{-Z})$$

$$C_1(Z) = -\frac{1}{3} + \frac{1}{Z^2} - \frac{3}{2Z^3} + e^{-Z}\left(\frac{5Z}{12} - \frac{3}{2Z} + \frac{5}{Z^3}\right) + e^{-2Z}\left(\frac{2}{3} - \frac{3}{Z^2} - \frac{7}{2Z^3} - \frac{2Z^2}{15}\right)$$

$$C_2(Z) = -\frac{1}{3} + \frac{1}{Z^2} - \frac{1}{Z^3} + \frac{e^{-Z}}{Z}\left(-\frac{1}{2} + \frac{1}{Z^2} + \frac{5Z^2}{24}\right)$$

Circular tube

$$C_3(Z) = \frac{1}{Z^2}\left[3 - \frac{2I_1(Z)}{ZI_0(Z)} - \frac{I_1^2(Z)}{I_0^2(Z)} - \frac{4I_1(Z)}{ZI_0(Z)}\right]$$

$$C_4(Z) = \frac{1}{Z^2}\left[1 - \frac{2I_1(Z)}{ZI_0(Z)}\right]$$

Table 2
Expressions for the functions $A(Z)$ and $B(Z)$ in the Nusselt number, Eq. (16)

	$A(Z)$	$B(Z)$
Parallel plate channel	$\frac{1}{12}-\frac{1}{2Z^2}+\frac{5}{8Z^3}-e^{-Z}\left(\frac{5Z}{48}-\frac{1}{2Z}+\frac{3}{2Z^3}\right)$ $+e^{-2Z}\left(-\frac{1}{6}+\frac{3}{4Z^2}+\frac{7}{8Z^3}+\frac{Z^2}{30}\right)$	$\frac{1}{12Z}-\frac{1}{4Z^2}+\frac{1}{8Z^3}+\frac{1}{4Z^4}$ $+e^{-Z}\left(-\frac{Z}{96}-\frac{5}{96}+\frac{1}{6Z}+\frac{1}{4Z^2}-\frac{1}{Z^3}-\frac{1}{2Z^4}\right)$ $+e^{-2Z}\left(\frac{7Z^2}{960}-\frac{5}{96}+\frac{1}{2Z^2}+\frac{7}{8Z^3}+\frac{1}{4Z^4}\right)$
Circular tubes	$\frac{1}{8}+\frac{1}{Z^2}\left[\frac{I_1^2(Z)}{I_0^2(Z)}+\frac{6I_1(Z)}{ZI_0(Z)}-3\right]$	$\frac{2}{Z^2}\left[\frac{I_1(Z)}{I_0(Z)}\left(\frac{1}{2}+\frac{Z}{8}\right)+\frac{I_1^2(Z)}{I_0^2(Z)}\left(\frac{1}{2}+\frac{2}{Z^2}\right)-1\right]$

will be explored over their full ranges in the results section to follow.

2.2.2. Constant wall temperature boundary condition

The differential equation governing thermal transport with uniform wall temperature is identical to that for the imposed constant wall heat flux, Eq. (8). However, the normalization for the temperature and nondimensional source are different, taking the more appropriate form $\theta=(T-T_w)/(T_m-T_w)$ and $S=sa^2/k(T_m-T_w)$. Also, for the thermally fully developed condition $\partial T/\partial x=-\theta(dT_m/dx)$. Neglecting axial conduction, the nondimensional energy equation thus becomes

$$\frac{1}{Y^n}\frac{d}{dY}\left(Y^n\frac{d\theta}{\partial y}\right)=-\theta U\left[\frac{\bar{u}a^2}{\alpha(T_m-T_w)}\frac{dT_m}{dx}\right]-S \qquad (17)$$

For an imposed constant wall temperature, there are two volumetric source scenarios deserving discussion. The first is $S=0$, which represents the traditional fully developed condition outlined in classical analytical treatments of convection heat transfer. The influence of axial conduction in this scenario has previously been explored for pressure-driven flow [37]. Given the implicit nature of Eq. (17) (since the term in the brackets on the right-hand side depends implicitly on the solution for θ), this problem was solved here numerically. In the case of $S=0$ and large Z, the classical slug flow problem which has appeared previously emerges, for which the fully developed Nusselt number is $Nu=9.869$ and $Nu=5.783$ [12] for the parallel plate channel and circular tubes, respectively. These values, as well as the classical results $Nu=7.541$ and 3.657 for pressure-driven flow in constant wall temperature parallel plate channels and circular tubes (with associated laminar flow, parabolic velocity profiles) were verified to within 0.1% in numerical solutions of this study. In order to characterize the limiting case of electro-osmotically generated flow in constant wall temperature channels with vanishing S, the electro-osmotic velocity profiles of Eqs. (4) and (5) were imposed in the numerical simulations. The resulting temperature profiles and corresponding Nusselt number were thus determined as a function of Z.

The second scenario of interest for channels of constant wall temperature is the asymptotic condition reached far downstream of the tube entrance. Under these conditions, the energy balance of Eq. (10) yields $dT_m/dx=0$, corresponding to the conditions $sa/q''_w=-2$ and -1 for the circular tube and parallel plate geometries, respectively. This interesting case is one for which all energy generated by volumetric heating in the fluid is dissipated convectively at the channel wall (resulting in fluid cooling). This situation is similar to fully developed Poiseuille flow in a tube with imposed constant wall temperature and viscous dissipation, studied by Ou and Cheng [38]. The asymptotic condition in that study also exhibited volumetric heating (represented by viscous heating—a nonuniformly distributed source in the wall-normal direction) which was dissipated at the channel wall. Since the volumetric energy generation in the fluid is assumed independent of axial position in the channel, an overall energy balance requires that there be axially uniform cooling of the fluid. The implication of this asymptotic condition is the existence of a (negative) uniform wall heat flux in a constant wall temperature channel. Recall that for uniform wall heat flux, $\partial^2T/\partial x^2=0$, and thus, axial conduction exerts no influence on the Nusselt number. It is unclear whether a thermally fully developed state satisfying Eq. (9) can exist in a constant wall temperature channel with volumetric heating prior to the establishment of the asymptotic $dT_m/dx=0$ condition described above. Given the very short thermal development length for typical electro-osmotically generated flows in microchannels, the question is perhaps only marginally relevant.

The solution for the fully developed temperature distribution and corresponding Nusselt number for the second volumetric scenario described above (for constant imposed channel wall temperature) may be found by integrating Eq. (17) analytically for the case $dT_m/dx=0$ (which mandates that $sa/q_w=-2$ and -1 for the circular tube and parallel plate configurations, respectively) to determine the temperature distribution. The mixed mean temperature is again determined for the value of Z of interest using Eq. (12). The resulting solution for the Nusselt number is identical to the solution for the constant wall heat flux boundary condition with $sa/q_w=-2$ (circular tube) and $sa/q_w=-1$ (parallel plates), where the fluid convective cooling at the wall is balanced by the volumetric generation. These solutions

are not repeated here, since they may be derived from Eq. (16) by specifying the appropriate value of S for the two configurations.

3. Discussion of thermal transport

Shown in Figs. 6 and 7 are the normalized temperature profiles $\theta = (T - T_m)/(q''_w a/k)$ for the constant heat flux condition in the parallel plate and circular tube geometries, respectively, plotted versus the wall-normal coordinate for several S values. Recall that $S = sa/q''_w$, and thus, for positive q''_w, S varies between 0 ($q''_w \to \infty$ or $s = 0$) and ∞ ($q''_w = 0$). Consequently, there exists no upper limit on the magnitude of θ. The $S = -2$ (circular tube) and -1 (parallel plates) cases correspond to the specified constant wall temperature solution where far downstream from the inlet, all of the energy generated due to the Joule heating is dissipated convectively at the tube walls, and thus, the fluid is cooled with a constant wall heat flux. The channel wall location corresponds to $Y = 0$ in Fig. 6 and $R = 1$ ($R = r/a$ for the circular tube) in Fig. 7, as shown in the coordinate system definitions of Fig. 2. Note that at $Z = 100$, θ is approaching a profile shape independent of S. Indeed for $Z \to \infty$, the velocity profile becomes uniform $U = 1$, and the dependence on S vanishes in Eq. (11). Resulting expressions describing θ can then be found through solution of the simplified, slug flow form of Eq. (11) (or, alternatively, by reducing Eqs. (13) and (14) for $Z \to \infty$). The limiting-case temperature profiles for $Z \to \infty$ are thus $\theta(Y) = Y^2/2 - Y + 1/3$ and $\theta(R) = (R^2 - 1)/2 + 1/4$ for the parallel plate and circular tube configurations, respectively. At the other velocity profile extreme for $Z \to 1$ the temperature profile shows significant dependence on S. Here, for increasing S (or increasing Joule heating), θ shows greater variation between the centerline and the wall temperatures. In general, the dependence of θ on S increases as Z decreases.

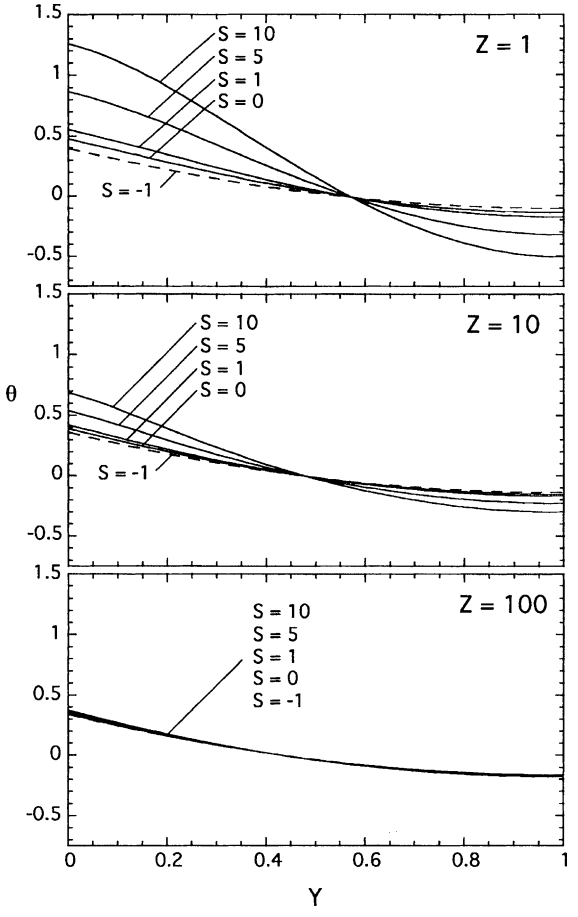

Fig. 6. Normalized temperature profiles for the parallel plate channel as a function of Z and S.

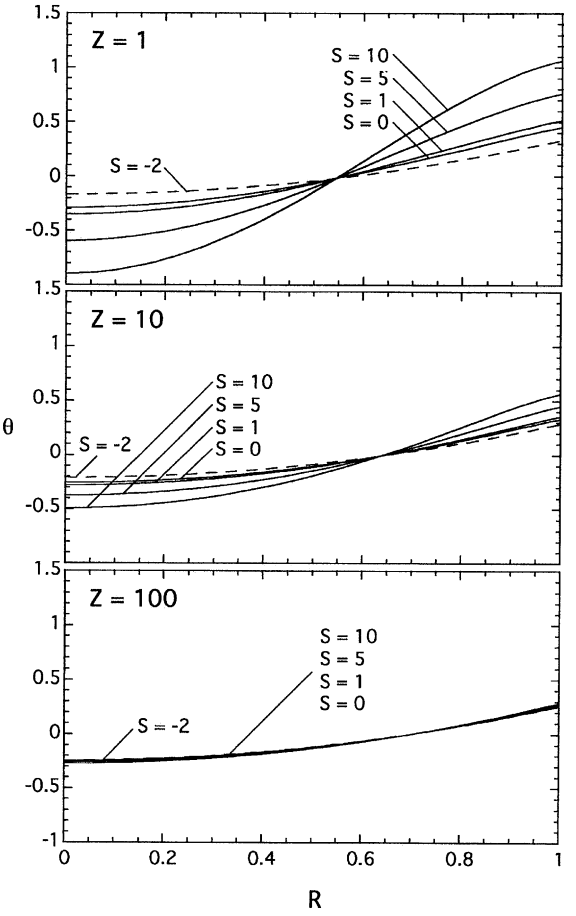

Fig. 7. Normalized temperature profiles for the circular tube as a function of Z and S.

The fully developed Nusselt number is plotted as a function of relative duct radius Z for values of S ranging from -1 to 100 and -2 to 100 in Figs. 8 and 9, respectively, for the parallel plate and circular tube geometries. As $Z \to \infty$, Nu approaches 12 and 8 for the two conditions, respectively, reproducing the results for slug flow. These values are independent of the magnitude of the internal energy generation, and as expected, the magnitude of Nu is greatest at this limiting condition. However, the value of Z at which Nu approaches its asymptotic value of 8 and 12 for the two geometries is dependent on S, observed to increase for increasing S. At the other extreme, as $Z \to 0.5$, the Nusselt number is strongly dependent on dimensionless source magnitude for the two geometries, and for the circular tube case the values are approximately the same as that for Poiseuille flow with internal volumetric heating as described by Tyagi [39]. Nu decreases as S increases for all finite values of Z. Indeed, for $S \to \infty$ (e.g., $q''_w \to 0$), the Nusselt number vanishes, $Nu \to 0$. At Z values between the extremes, where the velocity profile is neither parabolic nor uniform, the normalized heat transfer coefficient changes accordingly.

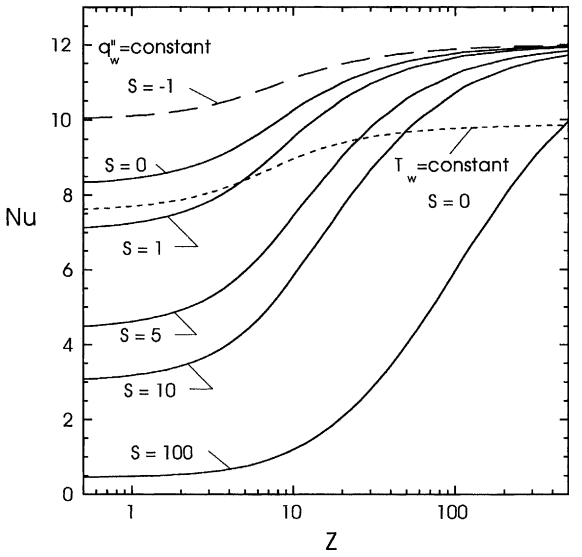

Fig. 8. Variation of the fully developed Nusselt number with Z and S for the parallel plate channel.

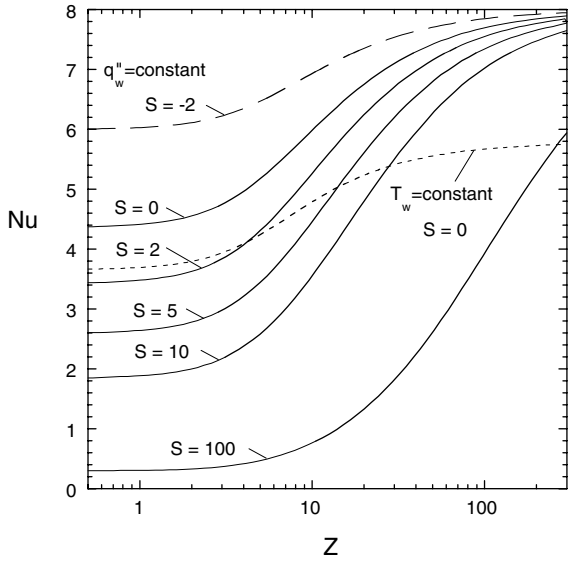

Fig. 9. Variation of the fully developed Nusselt number with Z and S for the circular tube.

Also shown in Figs. 8 and 9 is the Nusselt number behavior for constant wall temperature and constant wall heat flux boundaries with $S = 0$. Although for any electro-osmotic flow $S \neq 0$, these cases are included for completeness and comparative purposes. For vanishing dimensionless source, the Nusselt number for the constant wall temperature case is lower than for the constant wall heat flux condition for all Z. Note that for $S = 0$, as $Z \to 0.5$, Nu approaches the classical values for pressure-driven flow in tubes and between plates, for both the constant heat flux and constant wall temperature boundary conditions. The differences in Nu between the two boundary conditions for $S = 0$ are 10% and 19% for the parallel plates and circular tube, respectively. By contrast, as $Z \to \infty$ the differences in Nu between the two conditions are 22% and 38%.

The second constant wall temperature case considered (q''_w = constant with $S = -2$ or -1) is that for which all energy generated volumetrically in the fluid is dissipated convectively at the wall, and thus, cooling of the fluid occurs at a constant (negative) wall heat flux. This interesting case exhibits Nusselt numbers of greater magnitude for all Z than any other condition, constant wall heat flux or constant wall temperature, zero or nonzero source, for both geometries. The relative difference in the magnitude of Nu between the fluid cooling and other cases vanishes for $Z \to \infty$ and is largest as $Z \to 0.5$. At $Z = 0.5$, the Nusselt number for $S = -2$ in the circular tube is about 70% greater than for its $S = 2$ counterpart, despite the fact that the magnitude (but not the sign) of the wall heat flux is the same for the two cases. Similarly, for the parallel plate configuration the Nusselt number for $S = -1$ is approximately 20% greater than for the $S = 1$ case. This is illustrated graphically in the normalized temperature profiles of Figs. 6 and 7, where for a given Z magnitude the temperature gradients at the channel wall are identical for all S values, but the wall temperature decreases as S decreases. Thus, for the electro-osmotic flow considered here with volumetric energy generation, fluid cooling always results in higher heat transfer coefficient than fluid heating, even for conditions of identical wall heat flux magnitude.

It should be noted that for $Z \to \infty$ the present results are valid regardless of the magnitude of the wall zeta potential. However, as Z decreases the analysis and results are valid only for low zeta potentials (less than about 25 mV) since the Debye–Hückel linearization was invoked. For these restrictions the present results provide the fully developed convective heat transfer coefficient for the entire range of problem parameters for electro-osmotically generated flow in microchannels with constant properties. For larger wall potentials and finite Z, however, Eqs. (2) and (3) are no longer valid, and the solution to the excess charge distribution and corresponding velocity profiles must be obtained from numerical solution. In general the electro-osmotic mobility is a function of the fluid temperature since the viscosity, zeta potential, and dielectric constant are all temperature dependent. Likewise the Debye length exhibits some temperature dependence. Consequently, the momentum and energy equations are coupled when property variation is accounted for. In this case a closed form solution may exist for some idealized temperature dependent behavior. However, in general the solution must be obtained by numerical methods.

4. Conclusions

Thermally fully developed, electro-osmotically generated transport has been analyzed for a parallel plate microchannel and circular microtube under imposed constant wall heat flux and constant wall temperature boundary conditions. For the constant heat flux boundary condition, the fully developed Nusselt number has been found to depend on the duct radius/Debye length/duct radius ratio and the dimensionless volumetric source, varying between the limits defined by small and large relative radius. Increasing dimensionless volumetric source (due to the Joule heating) results in a decrease in Nusselt number for all relative channel sizes. For the constant wall temperature boundary condition, the channel streamwise asymptotic condition is one for which all energy generated volumetrically in the fluid due to Joule heating is dissipated convectively at the channel wall. This gives rise to a condition of simultaneous uniform wall temperature and uniform wall heat flux (with fluid cooling) in the fully developed region. This scenario is shown to be identical to the case of imposed constant wall heat flux with a negative dimensionless volumetric source whose magnitude is dictated by an overall fluid energy balance.

References

[1] P. Gravensen, J. Branebjerg, O.S. Jensen, Microfluidics–A review, J. Micromech. Microeng. 3 (1993) 168–182.
[2] S. Shoji, S. Nakagawa, M. Esashi, Micropump and sample injector for integrated chemical analysis systems, Sens. Actuators, A 21 (1990) 189–1192.
[3] B.H. van der Schoot, A. van den Berg, S. Jeanneret, N.F. de Rooij, A miniaturized chemical analysis system using two silicon micropumps, in: Transducers, 1991, pp. 789–791.
[4] L. Bousse, C. Cohen, T. Nikiforov, A. Chow, A.R. Kopf-Sill, R. Dubrow, J.W. Parce, Electrokinetically controlled microfluidic analysis systems, Annu. Rev. Biophys. Biomol. Struct. 29 (2000) 155–181.
[5] Z. Shulin, Fabrication and characterization of electrokinetic micro-pumps, Thermomechanical Phenomena in Electronic Systems—Proceedings of the Intersociety Conference 2 (2000) 31–36.
[6] C.T. Culbertson, R.S. Ramsey, J.M. Ramsey, Electro-osmotically induced hydraulic pumping on microchips: differential ion transport, Anal. Chem. 72 (2000) 2285–2291.
[7] P.K. Dasgupta, L. Shaorong, Electroosmosis: a reliable fluid propulsion system for flow injection analysis, Anal. Chem. 66 (1994) 1792–1798.
[8] N.A. Polson, M.A. Hayes, Electro-osmotic flow control of fluids on a capillary electrophoresis microdevice using an applied external voltage, Anal. Chem. 72 (2000) 1088–1092.
[9] S. Arulanandam, L. Dongqing, Liquid transport in rectangular microchannels by electro-osmotic pumping, Colloids Surf. A 161 (2000) 89–102.
[10] F.F. Reuss, Charge-induced flow, Proceedings of the Imperial Society of Naturalists of Moscow 3 (1809) 327–344.
[11] R.F. Probstein, Physicochemical Hydrodynamics, second ed., Wiley, New York, 1994.
[12] L.C. Burmeister, Convective Heat Transfer, Wiley and Sons, New York, 1983.
[13] R.J. Yang, L.M. Fu, C.C. Hwang, Electroosmotic entry flow in a microchannel, J. Colloid Interf. Sci. 244 (2001) 173–179.
[14] C.L. Rice, R. Whitehead, Electrokinetic flow in a narrow cylindrical capillary, J. Phys. Chem. 69 (1965) 4017–4024.
[15] D. Burgreen, F.R. Nakache, Electrokinetic flow in ultrafine capillary slits, J. Phys. Chem. 68 (1964) 1084–1091.
[16] S. Levine, J.R. Marriott, G. Neale, N. Epstein, Theory of electrokinetic flow in fine cylindrical capillaries at high zeta-potentials, J. Colloid Interf. Sci. 52 (1974) 136–149.
[17] T.L. Sounart, J.C. Baygents, Electrically-driven fluid motion in channels with streamwise gradients of the electrical conductivity, Colloids Surf. A 195 (2001) 59–75.
[18] C. Yang, C.B. Ng, V. Chan, Transient analysis of electroosmotic flow in a slit microchannel, J. Colloid Interf. Sci. 248 (2002) 524–527.
[19] S. Arulanandam, D. Li, Liquid transport in rectangular microchannels by electroosmotic pumping, Colloids Surf. 161 (2000) 29–102.
[20] L. Ren, D. Li, Electroosmotic flow in heterogeneous microchannels, J. Colloid Interf. Sci. 243 (2001) 255–261.
[21] J.P. Gleeson, Electroosmotic flows with random zeta potential, J. Colloid Interf. Sci. 249 (2002) 217–226.
[22] D.W. Arnold, P.H. Paul, Fluorescence-based visualization of electro-osmotic flow in microfabricated systems, Pro-

ceedings of SPIE—The International Society for Optical Engineering, Bellingham, WA 3877 (1999) 174–179.
[23] P.H. Paul, M.G. Garguilo, D.J. Rakestraw, Imaging of pressure- and electrokinetically driven flows through open capillaries, Anal. Chem. 70 (1998) 2459–2467.
[24] J.A. Taylor, E.S. Yeung, Imaging of hydrodynamic and electrokinetic flow profiles in capillaries, Anal. Chem. 65 (1993) 2928–2932.
[25] D. Ross, T.J. Johnson, L.E. Locascio, Imaging of electro-osmotic flow in plastic microchannels, Anal. Chem. 73 (2001) 2509–2515.
[26] T. Tsuda, M. Ikedo, Observation of flow profiles in electroosmosis in a rectangular capillary, J. Chromatogr. 632 (1993) 201–207.
[27] E.B. Cummings, PIV measurement of electro-osmotic and pressure-driven flow components in microfluidic systems, in: Microelectromechanical Systems (MEMS), MEMS-Vol. 1, ASME, 1999, pp. 377–382.
[28] C. Yang, D. Li, J.H. Masliyah, Modeling forced liquid convection in rectangular microchannels with electrokinetic effects, Int. J. Heat Mass Transf. 41 (1998) 4229–4249.
[29] C. Yang, D. Li, Analysis of electrokinetic effects on the liquid flow in rectangular microchannels, Colloids Surf. 143 (1998) 335–339.
[30] G.M. Mala, D. Li, J.D. Dale, Heat transfer and fluid flow in microchannels, Int. J. Heat Mass Transf. 40 (1997) 3079–3088.
[31] L.N. Tao, The second fundamental problem in heat transfer of laminar forced convection, J. Appl. Mech. 415–420 (1962).
[32] L.N. Tao, On some laminar forced-convection problems, ASME J. Heat Transf. 83 (1961) 466–472.
[33] W.A. Gobie, C.F. Ivory, Thermal model of capillary electrophoresis and a method for counteracting thermal band broadening, J. Chromatogr. 516 (1990) 191–210.
[34] J.H. Knox, Thermal effects and band spreading in capillary electro-separation, Chromatographia 26 (1988) 329–337.
[35] M.A. Bosse, P. Arce, Role of Joule heating in dispersive mixing effects in electrophoretic cells: convective-diffusive transport aspects, Electrophoresis 21 (2000) 1026–1033.
[36] T.E. Valko, H. Siren, M. Riekkola, Characteristics of electro-osmotic flow in capillary electrophoresis in water and in organic solvents without added ionic species, J. Microcolumn Sep. 11 (1999) 199–208.
[37] M.L. Michelsen, J. Villadsen, The Graetz problem with axial heat conduction, Int. J. Heat Mass Transf. 17 (1974) 1391–1402.
[38] J.W. Ou, K.C. Cheng, Viscous dissipation effects on thermal entrance heat transfer in laminar and turbulent pipe flows with uniform wall temperature, ASME Paper No. 74-HT-50, ASME, New York, 1974.
[39] V.P. Tyagi, Laminar forced convection of a dissipative fluid in a channel, ASME J. Heat Transf. 88 (1966) 161–169.